PHYSICAL REVIEW B **75**, 155331 (2007)

Ab initio calculations of the optical properties of the Si(113) 3×2 adatom-dimer-interstitial surface

K. Gaál-Nagy* and G. Onida

European Theoretical Spectroscopy Facility (ETSF), CNISM-CNR-INFM and Dipartimento di Fisica dell' Università degli Studi di Milano, via Celoria 16, I-20133 Milano, Italy

(Received 5 November 2006; revised manuscript received 19 January 2007; published 25 April 2007)

We investigated the stable silicon (113) surface with a 3×2 adatom-dimer-interstitial reconstruction by *ab initio* methods. The ground-state properties have been obtained using density-functional theory. We present the dispersion of the electronic band structure, where the surface bands have been distinguished from the projected bulk bands by calculating their localization in the slab. The optical spectra, here the reflectance anisotropy spectra (RAS), have been obtained within the independent-particle random-phase approximation. We identified surface features in the spectra, tracing them back to the responsible electronic states, and studied their localization in the slab. Theoretical results for the band structure and the RAS are compared with available experimental data.

DOI: 10.1103/PhysRevB.75.155331 PACS number(s): 78.68.+m, 68.35.Bs, 73.20.At

I. INTRODUCTION

Although of high index, the vicinal Si(113) surface is one of the stable silicon (Si) surfaces.[1] This surface is of technological interest, since atomically smooth and ultrathin oxide films can be grown on it.[2] Hence, it is considered as a candidate for the next generation of wafers,[3] and has potential applications in nanostructure technology. Si(113) can be used as a substrate for the self-assembled growth of germanium (Ge) nanodots[4] and nanowires,[5–7] as well as Ge (Refs. 8 and 9) and SiGe (Ref. 10) islands. Besides the technological issues, Si(113) is also of fundamental interest, because it shows phase transitions between its 3×2 and 3×1 reconstructions. These phase transitions can be induced by temperature[11–16] and by contamination.[17–24] The latter also affects the discussion about the surface reconstruction. In spite of the measurement of a 3×1 reconstruction,[25] most of the experiments show at room temperature (RT) a 3×2 surface periodicity.[4,13,17,18,20,26–29] The finding of the 3×1 periodicity might be due to contamination,[17] and the 3×2 one is assumed to be the surface unit of clean Si(113) at RT.

Various surface reconstructions have been proposed for the Si(113)3×2 surface. The most probable surface model is the adatom-dimer-interstitial (ADI) reconstruction of Dąbrowski *et al.*,[30] which is in agreement with experimental high-resolution transmission electron microscopy[31,32] and scanning tunneling microscopy[4,13,26,27,30,33] (STM) images. It has been confirmed by other theoretical investigations, too.[33–36] A top view of the surface unit cell is shown in Fig. 1. The surface reconstruction shows two adatoms, and two pentagons with a dimer along the $[1\bar{1}0]$ direction, with one pentagon hosting an interstitial atom in its center.

Earlier structural models were based on the geometry proposed by Ranke,[37] Si(113)3×1AD, which is similar to the ADI geometry. It can be deduced from the ADI model by eliminating the interstitial atom and relaxing the atoms in the z direction. Despite being intrinsically 3×1, in the 3×1AD model the 3×2 periodicity can also be obtained either by canceling one pentagon in each 3×2 surface unit cell ("surface void"[37]), or by manipulating the z coordinates of the pentagons in order to break the symmetry ("corrugated,"[38] "puckered,"[28,39] "shifted,"[40] etc.). Since the 3×1 periodicity is also interesting for the phase transition, being the periodicity of the high-temperature phase, besides the 3×1AD model also a 3×1AI one, with an interstitial atom at each pentagon, has been proposed.[33,41] However, other surface models have also been assumed, generally based on the models of Ranke or Dąbrowski *et al.*[42,43]

From the theoretical point of view the most stable surface (i.e., the one with the lowest surface energy) should be selected. For some of the models above the surface energy has been calculated, unfortunately by using different methods. There exist some studies assuming more than one surface reconstruction[30,33,35,36,44,45] within the same framework, but none of them considered all available surface models for comparison. Most of the calculations have shown that the Si(113)3×2ADI surface has the lowest surface energy with respect to the other assumed reconstructions.

Nevertheless, not all measurements agree with the ADI model.[28,31,40] The main criticism of the ADI model is due to the presence of a mirror plane, which should yield the extinction of some diffraction reflections,[43] because the corresponding patterns have been seen in some experiments.[46] Thus, models different from the ADI one are also being considered and a final conclusion has not been drawn yet.

An alternative approach for surface investigations is given by the study of their optical properties. A very efficient technique is reflectance anisotropy spectroscopy (RAS), which can be used *in situ* for surface characterization. The interpretation of such spectra is a demanding task. For this purpose it is necessary to have theoretical reference data, together with a correlation of the spectral features and the surface reconstruction elements.

The RAS of the Si(113) surface was measured ten years ago.[47,48] The first theoretical investigations of the RAS for the Si(113) surface were performed in 1998 by using a dipole approximation for the ideal bulk atomic positions.[49] In the same year, a tight-binding calculation was done for the Si(113)3×2ADI model,[50] where the bulk-derivative-like peaks were found with the wrong sign. Although tight-

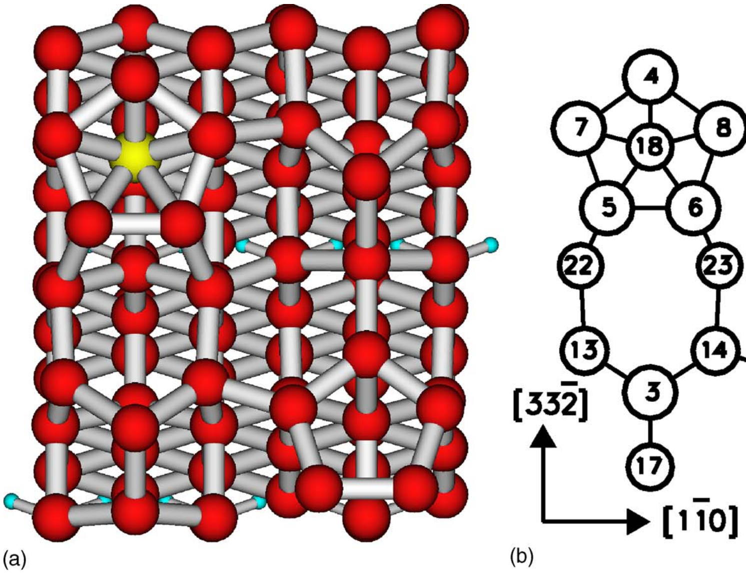

FIG. 1. (Color online) Top view of the Si(113)3×2ADI cell (x-y plane corresponding to [1$\bar{1}$0] and [33$\bar{2}$], respectively). Silicon atoms are large dark spheres (red). The interstitial Si atom (atom 18) is depicted as a large light (yellow) sphere. Hydrogen atoms are small light spheres (blue). For a side view see Figs. 5 and 8. Surface atoms (see sketch) include two pentagons with dimers (atom pairs 1-2 and 5-6) and two adatoms (atoms 3 and 9).

binding calculations yield good results for bulk silicon, the low-energy range of the spectrum, which is related to the surface, is usually not described very well.[51]

For this purpose, we choose an *ab initio* approach to investigate the optical properties of the Si(113) surface. The goal of this study is to find out whether surface-related structures in the spectrum can be traced back to some characteristic surface reconstruction elements of Si(113)3×2ADI (pentagons, interstitial, adatoms, etc.), and what kind of changes can be predicted with respect to other surface models. In this way optical spectroscopy could be used to discriminate between different models of reconstruction of the Si(113) surface. Due to the wide acceptance of Si(113)3 ×2ADI, we used this model as a starting point.

This paper is organized as follows. After summarizing briefly the methods used for the calculation (Sec. II), we first focus on the ground-state properties (Sec. III). Since the optical spectra are determined by the electronic transitions, an investigation of the electronic structure is presented in Sec. IV. A detailed discussion of the optical spectra is given in Sec. V, and, finally, we summarize and draw a conclusion.

II. METHOD

We have performed *ab initio* total energy calculations using the periodic slab method within the framework of the density-functional theory[52] as implemented in the ABINIT (Ref. 53) and TOSCA (Ref. 54) packages. For the exchange-correlation term in the Kohn-Sham equations[55] the local-density approximation[56,57] has been chosen. The eigenfunctions have been expanded into plane waves using pseudopotentials, here norm-conserving ones in the Troullier-Martins style.[58]

After converging the ground-state structure with ABINIT, the optical properties have been calculated using the TOSCA package.[54] The probability $P^{j}_{v\mathbf{k},c\mathbf{k}}$ of the electronic transitions between the valence (v) and conduction (c) states with electronic eigenenergies $E_{c\mathbf{k}}$ and $E_{v\mathbf{k}}$ for light polarized in the j ($j=x,y,z$) direction at a given point $\mathbf{k}$ in the reciprocal space has been calculated as the diagonal elements of the velocity operator.[59] Working within the independent-particle random-phase approximation[60] (IPRPA), local-field, self-energy, and excitonic effects are neglected. For our system we assume that they can be well described by the scissor operator approach;[61] hence we stick to the IPRPA to describe the optical properties. In order to obtain the RAS, in a first step the imaginary part of the slab polarizability α^{s} has been calculated as

$$\mathrm{Im}[4\pi\alpha^{\mathrm{s}}_{jj}(\omega)] = \frac{8\pi^2 e^2}{m^2\omega^2 A}\sum_{\mathbf{k}}\sum_{v,c}|P^{j}_{v\mathbf{k},c\mathbf{k}}|^2\delta(E_{c\mathbf{k}}-E_{v\mathbf{k}}-\hbar\omega) \tag{1}$$

for an energy ω.[62] Here, A is the surface area, and m and e the electron mass and charge, respectively. In order to smooth the resulting spectra, a Gaussian broadening has been applied, because it leads to better-defined structured spectra than the Lorentzian one. The RAS is defined as the difference of the deviation from the Fresnel reflectivity $\Delta R_j/R$ for the orthogonal polarizations within the surface plane (here the x and y directions):

$$I_{\mathrm{RAS}} = \frac{\Delta R}{R} = \frac{\Delta R_x}{R} - \frac{\Delta R_y}{R}. \tag{2}$$

The deviation from the Fresnel reflectivity for normally incident light is given by[62]

$$\frac{\Delta R_j}{R} = 4\left(\frac{\omega}{c_0}\right)\mathrm{Im}\left(\frac{\alpha^{\mathrm{surf}}_{jj}(\omega)}{\alpha_{\mathrm{b}}(\omega)}\right), \tag{3}$$

where $\alpha^{\mathrm{surf}}_{jj}$ is the complex surface polarizability and $\alpha_{\mathrm{b}}(\omega)$ the bulk one (c_0 is the velocity of light). The surface polarizability can be obtained by subtracting the bulk contribution from the slab one. Since the imaginary part is taken from the ratio, the bulk part in the numerator vanishes, and Eq. (3) holds for α^{s}_{jj} as well as $\alpha^{\mathrm{surf}}_{jj}$. The complex polarizability function α is derived from the imaginary part via the Kramers-Kronig transform.

Finally, to take into account the self-energy and excitonic effects in an approximate way, a scissor operator shift[61] has been applied to the eigenenergies.

III. GROUND STATE

For our calculations we have chosen the cell with the 3 × 2ADI surface reconstruction as described above. We have used slabs with 11 and 7 double layers (DLs) of Si, respectively. The amount of vacuum was taken equal to the slab thickness. Each DL consists of 12 Si atoms; just the surface DL contains one atom less. Since the slab is not symmetric, the dangling bonds at the bottom of the slab have been saturated with hydrogen (H). Therefore, the cells contain 131 or 83 Si atoms, respectively, and 18 H atoms. A top view of the slab is shown in Fig. 1, while the side views of the 11-DL cell can be seen in Figs. 5 and 8.

The convergence of the total energy requires four Monkhorst-Pack[63] **k** points in the irreducible wedge of the Brillouin zone (IBZ), and a kinetic-energy cutoff of 16 Ry. With these parameters, the error in the total energy is less than 0.046 eV per atom.

A relaxation of the topmost six DLs, computing the forces acting on the atoms (the remaining DLs have been kept fixed to bulk positions) shows significant changes with respect to the bulk positions just in the topmost four DLs. Therefore, these four DLs were optimized until the forces are less than 0.08 eV/Å.

We have calculated the surface energy by subtracting the energy of the hydrogenated surface and the bulk energy from the energy of the slab. The resulting value of 12.74 eV per unit cell agrees very well with the value of 12.69 eV obtained in Ref. 36. As a consequence, the value of surface energy per unit area of 87.87 meV/Å^2 is in good agreement with that of Stekolnikov *et al.*[36] (87.36 meV/Å^2). However, it is slightly lower than the ones obtained by other groups [97 meV/Å^2,[30,33] 90.4 meV/Å^2,[35] 94.8 meV/Å^2 (Ref. 45)] using various methods. Nevertheless, it is lower than that for other surface reconstructions and the overall agreement is good.

IV. ELECTRONIC STRUCTURE

After the ground state has been converged, a first step toward the optical properties is an analysis of the electronic structure. We started with the calculation of the electronic density of states (DOS) as displayed in Fig. 2, where the top of the highest occupied molecular orbital (HOMO) is set to 0 eV. We show in the same figure a comparison of the DOSs calculated with the 7-DL and the 11-DL slabs. The DOS has been obtained using a Brillouin-zone summation over 25 **k** points, together with a Gaussian broadening of 0.06 eV. The general shape is similar to that of bulk silicon for the occupied bands. In addition, around the energy gap surface-related structures are visible: one strong peak at the conduction band edge and a peak with a shoulder and another shoulder close to the bulklike part of the DOS at the valence band edge. The differences in the bulk-related structure of the DOS are due to the use of different slab cells.

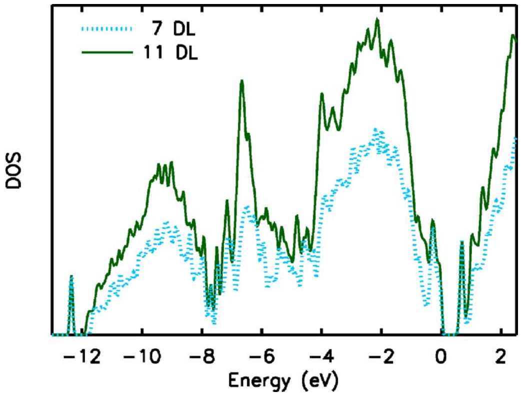

FIG. 2. (Color online) Electronic density of states for the 11-DL (solid dark-green lines) and the 7-DL cell (dotted light-blue lines). The zero of the energy scale is set to the top valence state. The height of the bulk-related part of the DOS reflects the thickness of the slab (see text).

The valence peaks around the Fermi energy, which are in addition to the bulk DOS, have also been found experimentally and they correspond to surface bands. Using angle-resolved ultraviolet photoemission spectra (ARUPS) Myler and Jacobi[18] found two peaks separated by 1.6 eV, where the second one is broad and could hide two single peaks. A similar experiment has been performed using angle-resolved photoelectron spectroscopy (ARPES) showing two single peaks separated by 0.4 eV, and a third one at lower energy with a nondispersive character, which is not resolved in the other experiment.[15,16,64] At normal emission, the two close peaks fall together, resulting in a single broad peak, which was found also by Myler and Jacobi.[18] Thus, the surface peak around the HOMO in the DOS is well defined in the experiments, and it contains probably two peaks as indicated by the shoulder. Furthermore, the core level spectra of Hwang *et al.*[15,16] were fitted using three surface peaks, where the second shoulder in our DOS might refer to that third peak. In scanning tunneling spectra[65] two peaks are visible. The low-energy maximum has been attributed to the tetramers and the high-energy maximum to the adatoms of the Si(113)3 × 2ADI reconstructed surface. For the peak at the lowest unoccupied molecular orbital which should be accessible by inverse photoelectron spectroscopy, no experimental results exist.

After identifying the surface structures in the DOS we have investigated the dispersion of the electronic eigenenergies using the 11-DL supercell. In order to separate the surface bands from the bulk background we have calculated the localization L_n for each state n by

$$L_n = \int d\mathbf{r}\, \psi^*_{n\mathbf{k}}(\mathbf{r})\,\theta(z)\,\psi_{n\mathbf{k}}, \tag{4}$$

where $\theta(z)$ is a real-space boxcar function,[66] meaning $\theta(z) = 1$ for a given range in the z direction and zero otherwise. $\psi_{n\mathbf{k}}$ is the single-band wave function for a given point **k** and the integral is taken over the whole supercell. Considering the range, e.g., from the subsurface DL to the vacuum above, the value of L_n corresponds to the integrated charge for that

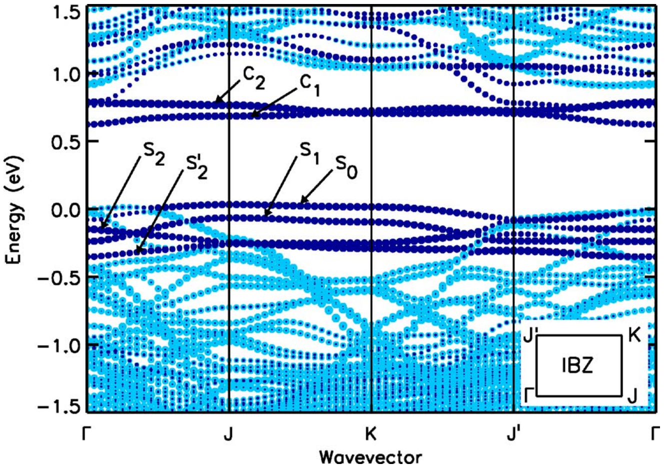

FIG. 3. (Color online) Dispersion of the electronic eigenenergies along the high-symmetry directions of the irreducible part of the Brillouin zone. According to the localization of the corresponding states in the slab, light dots correspond to bulk states and dark ones to surface states. The dot size accords with the value obtained by Eq. (4) (see text).

state located in the x-y slice with the chosen z range. In this way, the value indicates the amount of localization in the range selected by $\theta(z)$.

Figure 3 shows the results. The surface-localized bands are drawn with dark symbols (the z range has been chosen to cover the topmost two DLs), and the bulk-localized bands with light symbols (the z range has been chosen to cover the lowest seven DLs where the relaxation has not changed the bulk positions). The sizes of the dots correspond to the amount of localization in this area. This means, e.g., for the topmost four valence bands at the Γ point, that the top band is less localized in the bulk area than the second one and the third band is less localized in the surface area than the fourth one.

With this procedure we have identified three surface valence bands (S_0, S_1, S_2) and two surface conduction bands (C_1, C_2), as shown in Fig. 3. All surface bands show a partial overlap with the bulk band structure. This points to a reduced influence of excitonic effects, and thus the IPRPA scissor approximation is expected to work well. The state S_2 appears as a state folded at J along the $[1\bar{1}0]$ direction, and hence shows a 3×1 periodicity. The other surface states show the 3×2 one. Of course, the eigenvectors have 3×2 symmetry for all surface states due to the choice of the 3×2 supercell. In the experiments by both ARUPS and ARPES, valence surface states with 3×1 and 3×2 periodicity were found, but with a larger energy difference, which is here between J and K at about 0.16–0.19 eV. The shapes of the bands S_1 and S_2 are in excellent agreement with the measured ones, and show similar dispersions of about 0.17 and 0.20 eV, respectively, compared with the experiments of An *et al.*[64] (S_1, 0.15 eV and S_2, 0.30 eV) and Myler and Jacobi[18] (S_1, 0.20 eV and S_2, 0.15 eV). Hence we conclude that these two states are the ones appearing in the experiments. Along the Γ-J direction the separation of the surface bands S_0 or S_1 and S_2 shows large variations within the two experiments, where we have an overlap of S_1 and S_2, and a separation of S_0 and S_2. Thus, our results are between the two experimental findings. The discrepancy might be due to the neglect of quasiparticle corrections as well as to experimental setups. Considering available theoretical investigations of the dispersion of the eigenenergies of the Si(113) surface (in addition to the tight-binding study of Wang *et al.*[39] using a puckered surface model, which is hence not comparable), there exists just the investigation of Stekolnikov *et al.*[36] Within their results they obtain also the surface states S_0 and S_1, where S_2 might be hidden in the bulk-projected band structure. The energy spacing between these states is similar to the one obtained here.

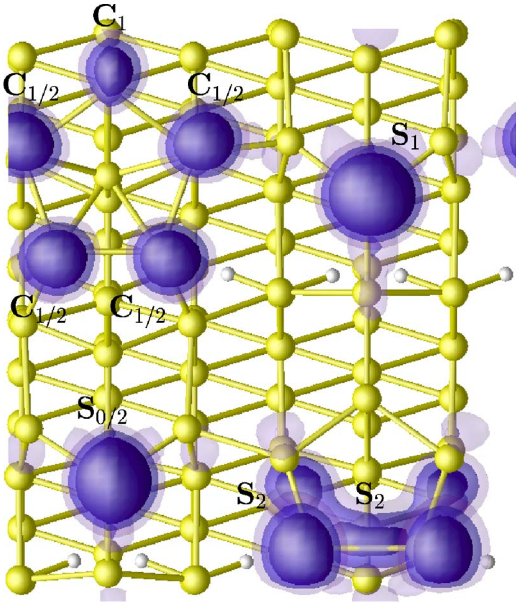

FIG. 4. (Color online) Top view (x-y side as in Fig. 1) of the Si(113)3×2ADI cell together with the charge density of the surface states S_0, S_1, S_2, C_1, and C_2 at the Baldereschi **k** point (see text). Note the overlap between the localization of some of the surface states.

By calculating the squared modulus of the wave functions of the surface states we have been able to localize them more precisely in the slab (see Fig. 4). The states S_0 and S_1 are located at the adatoms (atom 3 and atom 9, respectively; see Fig. 1) and show a dangling bond character, which is in agreement with the results of Ref. 36 and the assumption of Ref. 65. The states C_1 and C_2 have been found at the atoms 4-7-8 and 5-6-7-8 of the pentagon with the interstitial, as stated similarly in Ref. 36. Furthermore, the surface state S_2 is located at one adatom and two atoms of the empty pentagon (atoms 1-2 and 3), which has not been investigated before. However, this was already assumed by Arabczyk *et al.*[65] Anyway, this state is also present in experimental[4,26,27,30,33,35] and theoretical[30,33,35,36] STM images.

In addition to the surface states above, we have obtained an additional valence surface state at very low energy corresponding to the separated peak at around −12.5 eV in the DOS of Fig. 2. This state shows a dispersion of less than 16 meV, which follows the dispersion of the lowest valence states, which is 20 times larger. Thus, this nearly flat state can be considered as a Tamm-like state.[67] This state is lo-

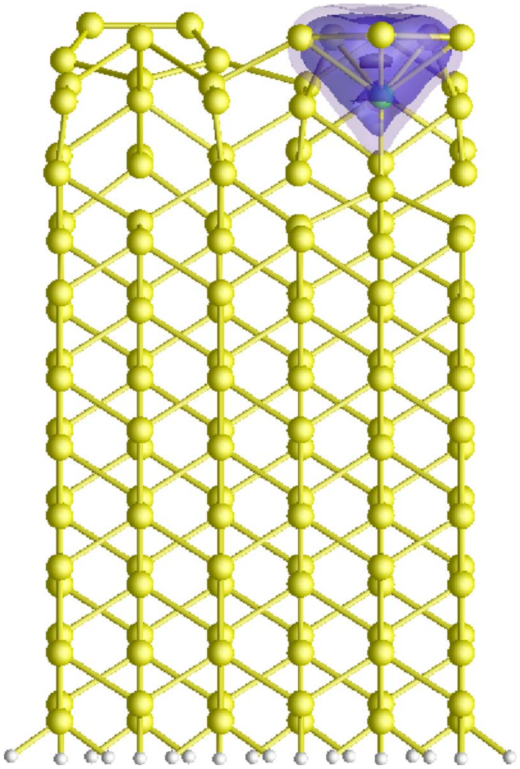

FIG. 5. (Color online) Side view (x-z plane) of the Si(113)3×2ADI cell together with the charge density of the low-energy Tamm-like state. This state is almost dispersionless, and it is represented here at the Baldereschi **k** point. Si atoms are drawn as large spheres, H atoms as small spheres.

cated in between the atoms of the pentagon with interstitial (atoms 4-5-6-7-8 and 18), as displayed in Fig. 5. The large separation between these sites in the real space is responsible for the flat character of the band. Low-lying flat surface states have been found in the past. Pandey *et al.*[68] found a flat surface band at low energy ($\approx$10.8 eV) which is partially below the bulk valence bands for Si(111):SiH$_3$. Also a theoretical and experimental investigation of the GaAs(110)1×1 surface[69] shows one surface state located at low energy. However, no surface state entirely below the valence band minimum was found. The Tamm-like state observed in our calculation should be experimentally accessible and its experimental finding would confirm the validity of the surface model used here. Due to its low-energy character, transitions from that state will not appear in the low- or middle-energy range of the RAS.

V. OPTICAL PROPERTIES

In this section we present results for the optical spectra, in particular for the RAS, of the Si(113) surface. We focus on the convergence with respect to the **k** points and the slab thickness, we analyze the RAS regarding surface contribution and responsible transitions, and we compare with available experimental results.

A. Convergence tests

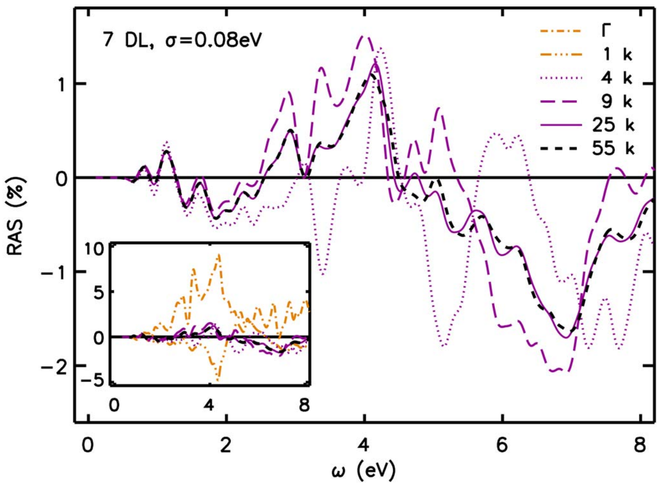

FIG. 6. (Color online) Convergence of the RAS of Si(113)3×2ADI with respect to the **k** point summations. The results for the one **k**-point sets (Γ and Baldereschi) are shown in the inset, since the corresponding RAS is larger by one order of magnitude. Convergence requires 25 **k** points in the IBZ (see text).

For the optical properties we have performed convergence tests concerning the number of conduction states and the number of **k** points used in Eq. (1). A number of 460 bands in total (189 conduction states) was sufficient for the 11-DL cell as well as 360 bands (185 conduction states) for the 7-DL one. Each state has been expanded into plane waves. The use of 4000 **G** vectors over the available set of $\approx$24 000 plane waves was enough for the convergence of the matrix elements. The convergence tests with respect to the special **k** points are more demanding. In our case, the **k** points can be chosen in one-quarter of the BZ, corresponding to the IBZ. A Gaussian broadening of 0.08 eV gives reasonably structured spectra. We have performed tests with various sets of **k** points for the 7-DL cell as shown in Fig. 6. As visible in the figure, up to 25 **k** points the spectra still show some deviations. With a single-**k** analysis[70] it has been figured out that the variations along the x direction in reciprocal space are larger than in y direction and thus an increase of the number of **k** points just in the x direction (resulting in a set of 55 **k** points) yields a strong improvement of the convergence. Comparing the spectra based on 25 and 55 **k** points we have concluded that convergence has already been achieved with 25 **k** points. Incidentally, using the Γ point only, a strong anisotropy appears (see inset of Fig. 6) which can be traced back to infinite chains in the x direction of the bulk layers.[70]

Since the slab thickness can influence the spectra, we have calculated the RAS using only the Baldereschi[71] point for various cell sizes, i.e., using slabs of 7, 11, and 15 DLs. The 15-DL cell has been created by adding four bulk DLs to the 11-DL slab. The outcome of the test is displayed in Fig. 7. It is clearly recognizable that the 7-DL slab does not describe the low-energy region of the RAS correctly, where the differences between the 11-DL and 15-DL cells are just minor ones. Also, for the medium- and high-energy range the spectral features are reproduced with the 11-DL cell, even if they are slightly underestimated. Hence, the use of the 11-DL cell produces reliable results for the surface spectra. Note that the spectra using only the Baldereschi point are not converged, but the use of just one point is sufficient for the

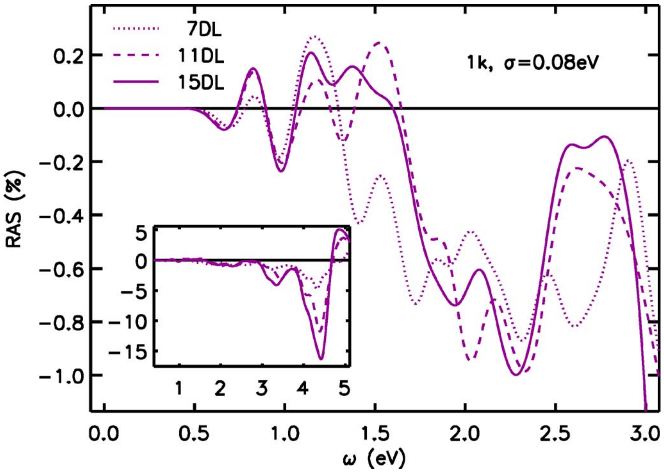

FIG. 7. (Color online) Convergence of the RAS of Si(113)3 $\times$2ADI with respect to the slab thickness (7, 11, and 15 DL) using only the Baldereschi point in Eq. (1). The spectra for an enlarged energy range are shown in the inset. Convergence is satisfactory using the 11-DL slab (see text).

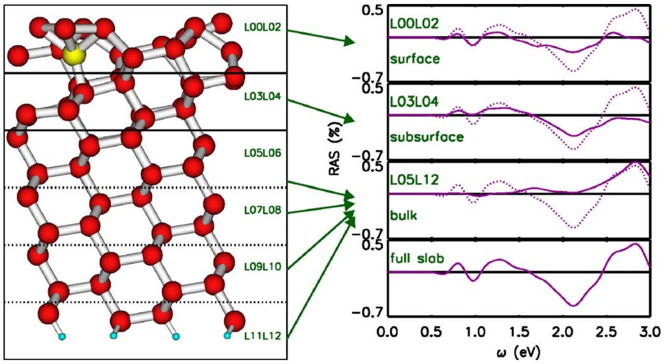

FIG. 8. (Color online) Side view of the 11-DL slab (left side) and layer-by-layer analysis of the RAS (right side). In addition to the decomposed spectra (solid lines) also the full spectra (dotted lines in the upper three panels and solid line in the lower one on the right) are drawn for comparison. The arrows indicate where the contributions to the spectra come from. The DL assignment is explained in the text.

check performed here. It has already been shown that the convergence regarding the thickness improves on using more **k** points.[72] Concerning the **k**-point convergence, we expect that our 25-**k**-point set, which has been shown to be enough for the 7-DL slab, will also be at convergence for the 11-DL one.

B. Analysis of the RAS

We proceed now to analyze our fully converged RAS (using the 11-DL supercell and 25 **k** points) with respect to the surface structure. Thus, we have performed a layer-by-layer decomposition as described in Refs. 66, 73, and 74. For this purpose, a real-space cutoff has been used in order to separate the contributions coming from defined layers of the slab by introducing a boxcar function $\theta(z)$ in the calculation of the dipole matrix elements. The modified transition probability $\tilde{P}^j_{v\mathbf{k},c\mathbf{k}}$ can be rewritten as

$$\tilde{P}^j_{v\mathbf{k},c\mathbf{k}} = -i\hbar \int d\mathbf{r}\, \psi^*_{v\mathbf{k}} \theta(z) \frac{\partial}{\partial r_j} \psi_{c\mathbf{k}} \tag{5}$$

and the summation of Eq. (1) changes to

$$\mathrm{Im}[4\pi\alpha^s_{jj}(\omega)] = \frac{8\pi^2 e^2}{m^2\omega^2 A} \sum_{\mathbf{k}} \sum_{v,c} [P^j_{v\mathbf{k},c\mathbf{k}}]^* \tilde{P}^j_{v\mathbf{k},c\mathbf{k}} \times \delta(E_{c\mathbf{k}} - E_{v\mathbf{k}} - \hbar\omega). \tag{6}$$

Note that only one of P and P^* must contain the θ function. The decomposed spectra are presented in Fig. 8 together with a side view of the slab. We have numbered the DLs from the top to the bottom. For the analysis we have chosen three regions: the topmost two DLs [DL01 and DL02 (surface), while DL00 is the vacuum layer above], the third and fourth DLs (subsurface, DL03 and DL04) where the optimization changed the atomic positions with respect to the bulk ones, and the bulk part together with the hydrogens (bulk, DL05–DL11, while DL12 is the vacuum layer below), since the relaxation did not affect the atomic positions in DL05 and DL06.

In the low-energy range of the spectra various peaks are visible. For further discussion we have labeled the low-energy peaks with $P1$, $P2$, $P3$, $P4$, and $P5$ (see Fig. 10 below). Looking at the decomposed spectra in Fig. 8 one can see that the peaks in the full spectra (containing the contribution of all DLs) up to 2.5 eV ($P1$–$P5$) can be traced back to the surface and the subsurface DLs, where the structures at higher energies are also bulk determined. Nevertheless, at energies larger than 3 eV there also exist surface-related structures. However, these structures are due to surface-bulk and bulk-surface transitions and surface resonances. $P1$ and $P3$ originate from the surface layers only, whereas the peaks $P2$, $P4$, and $P5$ contain contributions from both the surface and the subsurface layers. Thus we can conclude that for an analysis of $P1$ and $P3$ only transitions between surface bands need to be considered, whereas for $P2$, $P4$, and $P5$ also resonances or high-energy bulk states have to be investigated.

After identifying the surface peaks in the spectra, we want to identify the responsible transitions. Since for the deviation from the Fresnel reflectivity Eq. (3) the whole complex polarizability is considered, the RAS is also influenced by the real part of α. Thus, an overlap of spectral structures coming from the imaginary and the real parts is possible. A feasible procedure for determining this overlap has been described in Ref. 75, where Eq. (3) was rewritten as

$$\frac{\Delta R_j}{R} = A\,\mathrm{Im}(4\pi\alpha^s_{jj}) + B\,\mathrm{Re}(4\pi\alpha^s_{jj}). \tag{7}$$

The energy-dependent coefficients A and B are determined only by the dielectric function of the bulk crystal. With the magnitude of A and B one can figure out if the RAS is mainly determined by $\mathrm{Im}(4\pi\alpha^s)$ or $\mathrm{Re}(4\pi\alpha^s)$. In this way, A and B are surface-independent coefficients.

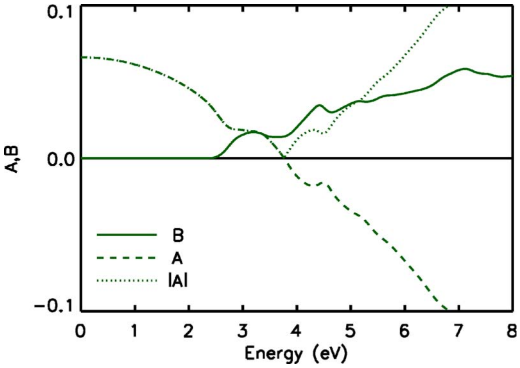

FIG. 9. (Color online) Bulk coefficients A and B from Eq. (7). For energies smaller than 2.5 eV there is no contribution of $\mathrm{Re}(4\pi\alpha^{s})$ to the RAS (see text).

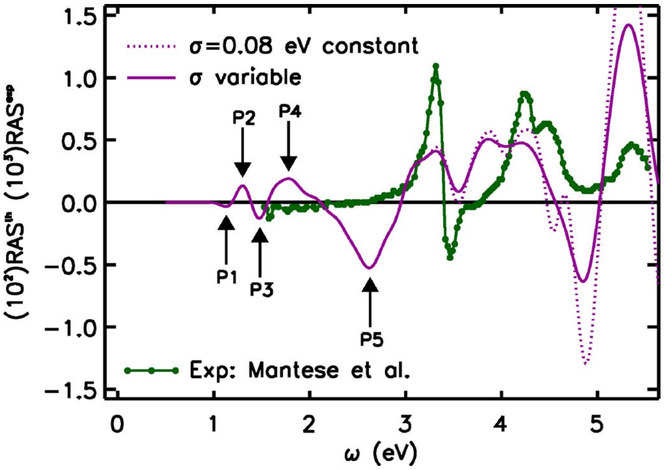

FIG. 10. (Color online) Comparison of the RAS calculated using 25 **k** points in the 11-DL cell (light curves) obtained with a constant broadening of 0.08 eV (dotted line) and a variable one (solid line); see text. The experimental spectra are from Refs. 47 and 48 (dark dots connected by a solid line). A scissor operator of 0.5 eV has been applied to the theoretical spectra, and the RAS amplitude has been scaled by a factor of 10 (see text).

We hence analyzed these coefficients for our system, i.e., we determined A and B for bulk silicon. They are universal for all silicon surfaces, independent of the orientation and reconstruction. The result is shown in Fig. 9. In addition to A and B, $|A|$ is also plotted in order to compare the magnitude of the coefficients. The result is the following. Every RAS of any clean silicon surface is determined only by $\mathrm{Im}(4\pi\alpha^{s})$ for an energy up to 2.5 eV and by both, $\mathrm{Im}(4\pi\alpha^{s})$ and $\mathrm{Re}(4\pi\alpha^{s})$, for higher energies. In detail, it is mainly determined by $\mathrm{Im}(4\pi\alpha^{s})$ for 2.5–3.2 eV, by both equally from 3.2–3.4 eV, mainly by $\mathrm{Re}(4\pi\alpha^{s})$ for 3.4–5.1 eV, and by $-\mathrm{Im}(4\pi\alpha^{s})$ for higher energies. Thus, the surface peaks $P1-P5$ can be traced back to the differences just between $\mathrm{Im}(4\pi\alpha^{s}_{xx})$ and $\mathrm{Im}(4\pi\alpha^{s}_{yy})$. These are the differences we investigate now in order to find the origin of the surface features in the RAS.

Since the RAS in the low-energy range (up to 1.3 eV, peaks $P1$ to $P3$) has been reproduced already sufficiently well using the Baldereschi point only, based on this spectrum the contribution of various transitions to the first three surface peaks has been analyzed. For the other spectral structures all **k** points have been taken into account.

The first peak $P1$ of the RAS displayed in Fig. 10 appears due to the transition from the surface valence state S_0 to the surface conduction state C_1. Considering the localization of the states (see Fig. 4), namely, the position of the adatom 3, where the charge density of S_0 has been found, and that of the atoms 4-7-8 (the location of C_1) one sees that they are much nearer in the y direction than in x. Therefore the transition probability in this case is higher for y-polarized light, resulting in a negative RAS signal. Note that the transition from S_0 to C_2 is forbidden. Also the peak $P2$ in the RAS is due to transitions between surface bands: the transitions from S_1 to both the surface conduction bands C_1 and C_2 are responsible for it. Here, the distance between adatom 9 (S_1) and the filled pentagon 4-5-6-7-8 (C_1 and C_2) in the x direction is small, where also a small overlap of the charge density appears. This yields a strong positive signal in the RAS. Note that due to the overlap of S_1 with the bulk bands there is also a tiny contribution of bulk-surface transitions to $P2$. The peak $P3$ is determined by transitions from S_2 to C_1 and C_2. The vicinity of the state S_2, which is located at atoms 1-2-3, to the states C_1 and C_2 at the pentagon with interstitial (4-5-6-7-8) is mainly due to its localization at adatom 3. From the charge density localized at the atoms 1-2 the transition probability should be similar for both polarizations since the distances in the x and y directions are equal. The additional localization at adatom 3 favors the y direction, yielding the negative RAS signal. For the remaining two peaks $P4$ and $P5$ a mixture of bulk-surface and surface-bulk transitions (not restricted to single surface bands) is responsible; therefore a clear picture could not be drawn. The peaks $P2$ and $P3$ are equal in height, whereas $P1$ is lower. This might be due to the fact that for $P2$ and $P3$ transitions to two surface conduction states are responsible, but one of them is forbidden for $P1$. However, the overall magnitude of the probability of single transitions between surface bands is nearly the same in this case.

Considering the dispersion of the eigenenergies, the regions in the IBZ with the main contributions to the RAS have been identified using again a single-**k** analysis:[70] For $P1$, **k** points near Γ carry the main contribution, whereas for $P2$ **k** points close to the J-K boundary (large k_x component), and for $P3$ those close to the Γ-J boundary (small k_y component) comprise the main contributions. Such a trend has not been found either for $P4$ or for $P5$. *A posteriori*, due to this anisotropic distribution of the contribution, the convergence with respect to the **k** points had to be expected to be a delicate one.

Changing the surface reconstruction certainly would affect the RAS. We can speculate that removing, e.g., the interstitial atom (atom 18) would change the localization of the states C_1 and C_2, which would have an effect on all three peaks discussed here. Adding an interstitial to the empty pentagon would affect mainly state S_2, meaning the third peak in the spectra. Furthermore, having two nearly equivalent pentagons on the surface would influence the peak height, because the transition probability for x and y would not be as significantly different as for the ADI reconstruction. However, the energetic position of the surface peaks would also be affected.

C. Comparison with experimental results

Finally, in Fig. 10 we compare our RAS with the experimental data obtained by Aspnes and co-workers.[47,48] Unfortunately, the measured RAS did not show any surface-related spectral structure. This might be due to passivation of the surface with Si-O suboxide. Thus, the theoretical surface peaks we have investigated cannot be compared. Regarding bulk-related structures, using an 11-DL slab does not allow the perfect description of the bulk-derivative-like structure. In order to wash out artificial oscillations of bulk-originated structures, we have applied a variable broadening. This means we have used a constant broadening $\sigma=0.08$ eV for energies smaller than 2.5 eV (onset of the bulk spectra) and an additional broadening which grows linearly with the energy (a factor of 0.04 in the energy difference $\omega-2.5$ eV) for higher energies. Furthermore, we scaled the measured RAS with a factor of 10, which is the usually accepted factor for silicon surfaces.[76] In this way we got a reasonable agreement with respect to our slab thickness in the medium-energy range. As visible, the calculation reproduces the spectral structure at around 3.2 eV and the double peak at 4.2 eV, which is shifted slightly to lower energies in our case. Also the experimental structure at around 5 eV can be found in our spectra; however, it is a little overestimated. The bulk-derivative-like structure itself at around 3.5 eV is reproduced only qualitatively, which is a result of the small slab size. Compared to the tight-binding calculation of Gavrilenko *et al.*,[50] our spectra can resolve the characteristic low-energy surface peaks and describes the bulk-derivative-like structure with the correct sign.

VI. SUMMARY AND CONCLUSIONS

In summary, we have investigated the electronic structure and the RAS of the Si(113)3×2ADI. The electronic band structure and the DOS were found in agreement with available experimental results. We identified three surface valence bands and two surface conduction bands near the Fermi level by computing the wave function localization in the surface region. The valence surface states are located at the adatoms and at the pentagon without an interstitial, whereas the conduction surface states are located at the pentagon with an interstitial, in agreement with STM images. The three valence surface states in the energy gap compare with the two states which are visible in ARUPS (Ref. 18) and ARPES (Refs. 15, 16, and 64) experiments; in the latter a third surface (resonance) state has also been found, in overlap with the bulk states. The existence of three surface valence states has been confirmed by the comparison of theoretical[30,33,35] and experimental[4,26,27,30,33,35] STM images and by a core-level analysis.[15,16] Two of the valence surface states show a 3×2 and one a 3×1 periodicity, which has been confirmed experimentally.[18,64] In addition, we found a surface state below the valence band minimum. This state is located at the filled pentagon and shows a Tamm-like character. This finding calls for more experimental work for measuring the DOS at low energy.

Concerning optical spectra, after checking the numerical convergence with respect to the slab thickness and the number of **k** points, we have performed a layer-by-layer spectral decomposition. In this way the surface-relevant spectral features have been determined. Furthermore, an analysis of the contributions of the real and imaginary parts of the polarizability leads to the conclusion that the surface-relevant structures are due to the imaginary part only. We have traced back the first three low-energy peaks of the RAS to transitions from the three valence surface states S_0, S_1, and S_2 (localized at the adatoms and the empty pentagon) to both the conduction surface states C_1 and C_2 (localized at the pentagon with interstitial). These RAS peaks are hence very sensitive to a change of the surface reconstruction. The missing splitting of the peaks in the RAS with respect to the two surface conduction states is due to the small energy difference between them. The only available experimental RAS does not show any low-energy surface-related spectral features, probably due to surface contamination. At higher energy, the bulk-derivative-like structure, as well as other spectral features, agree with those of the measured RAS. Differences with respect to the experimental results might be due to the limited size of the slab used in the calculations, and to the neglect of self-energy and excitonic effects.

ACKNOWLEDGMENTS

This work was funded by the EU's Sixth Framework Program through the NANOQUANTA Network of Excellence (Grant No. NMP4-CT-2004-500198). We would like to thank A. Incze, C. Hogan, and R. Del Sole for fruitful discussions. K.G.N. also wants to thank S. Hinrich for providing articles and additional information about the Si(113) surface. Computer facilities at CINECA granted by INFM (Projects No. 352/2004 and No. 426/2005) are gratefully acknowledged.

---

*Electronic address: katalin.gaal-nagy@physik.uni-r.de

[1] D. J. Eaglesham, A. E. White, L. C. Feldman, N. Moriya, and D. C. Jacobson, Phys. Rev. Lett. **70**, 1643 (1993).

[2] H.-J. Müssig, J. Dąbrowski, and S. Hinrich, Solid-State Electron. **45**, 1219 (2001).

[3] H.-J. Müssig, J. Dąbrowski, K.-E. Ehwald, P. Gaworzewski, A. Huber, and U. Lambert, Microelectron. Eng. **56**, 195 (2001).

[4] Z. Zhang, K. Sumitomo, H. Omi, T. Ogino, and X. Zhu, Surf. Interface Anal. **36**, 114 (2004).

[5] M. P. Halsall, H. Omi, and T. Ogino, Appl. Phys. Lett. **81**, 2448 (2002).

[6] Z. Zhang, K. Sumitomo, H. Omi, and T. Ogino, Surf. Sci. **497**, 93

(2002).
[7] K. Sumitomo, Z. Zhang, H. Omi, D. J. Bottomley, and T. Ogino, J. Cryst. Growth **237-239**, 1904 (2002).
[8] J. Knall and J. B. Pethica, Surf. Sci. **265**, 156 (1992).
[9] H. Omi and T. Ogino, Phys. Rev. B **59**, 7521 (1999).
[10] M. Hanke, T. Boeck, A.-K. Gerlitzke, F. Syrowatka, and F. Heyroth, Appl. Phys. Lett. **86**, 223109 (2005).
[11] Y.-N. Yang, E. D. Williams, R. L. Park, N. C. Bartelt, and T. L. Einstein, Phys. Rev. Lett. **64**, 2410 (1990).
[12] Y. R. Xing, J. P. Zhang, J. A. Wu, C. Z. Liu, and C. H. Wang, Surf. Sci. **232**, L215 (1990).
[13] H. Hibino and T. Ogino, Phys. Rev. B **56**, 4092 (1997).
[14] T. Suzuki, H. Minoda, Y. Tanishiro, and K. Yagi, Surf. Rev. Lett. **5**, 249 (1998).
[15] C. C. Hwang, H. S. Kim, Y. K. Kim, K. W. Ihm, C. Y. Park, K. S. An, K. J. Kim, T. -H. Kang, and B. Kim, Phys. Rev. B **64**, 045305 (2001).
[16] C. C. Hwang, K.-J. Kim, T.-H. Kang, B. Kim, Y. Chung, and C. Y. Park, Surf. Sci. **514**, 319 (2002).
[17] K. Jacobi and U. Myler, Surf. Sci. **284**, 223 (1993).
[18] U. Myler and K. Jacobi, Surf. Sci. **220**, 353 (1989).
[19] Y.-N. Yang and E. D. Williams, J. Vac. Sci. Technol. B **8**, 2481 (1990).
[20] S. M. Scholz and K. Jacobi, Phys. Rev. B **52**, 5795 (1995).
[21] C. C. Hwang *et al.*, J. Vac. Sci. Technol. A **18**, 1473 (2000).
[22] H. Kim, T. Spila, and J. E. Greene, Surf. Sci. **490**, L602 (2001).
[23] Z. H. Zhang, K. Sumitomo, and F. Lin, Ultramicroscopy **105**, 16 (2005).
[24] Z. H. Zhang and K. Sumitomo, Surf. Sci. **576**, 83 (2005).
[25] M. J. Hadley, S. P. Tear, B. Rottger, and H. Neddermeyer, Surf. Sci. **280**, 258 (1993).
[26] J. Knall, J. B. Pethica, J. D. Todd, and J. H. Wilson, Phys. Rev. Lett. **66**, 1733 (1991).
[27] H. Sakama, D. Kunimatsu, M. Kageshima, and A. Kawazu, Phys. Rev. B **53**, 6927 (1996).
[28] C. Y. Chang, Y. C. Chou, and C. M. Wei, Phys. Rev. B **59**, R10453 (1999).
[29] C. C. Hwang, H. S. Kim, Y. K. Kim, J. S. Kim, C. Y. Park, K. J. Kim, T.-H. Kang, and B. Kim, Phys. Rev. B **59**, 14864 (1999).
[30] J. Dąbrowski, H.-J. Müssig, and G. Wolff, Phys. Rev. Lett. **73**, 1660 (1994).
[31] I. Takeguchi, M. Tanaka, H. Yasuda, and K. Furuya, Surf. Sci. **482-485**, 1385 (2001).
[32] M. Takeguchi, Y. Wu, and K. Furuya, Surf. Interface Anal. **30**, 288 (2000).
[33] J. Dąbrowski, H.-J. Müssig, and G. Wolff, J. Vac. Sci. Technol. B **13**, 1597 (1995).
[34] J. Dąbrowski, H.-J. Müssig, and G. Wolff, Surf. Sci. **331-333**, 1022 (1995).
[35] G.-D. Lee and E. Yoon, Surf. Sci. **559**, 63 (2004).
[36] A. A. Stekolnikov, J. Furthmüller, and F. Bechstedt, Phys. Rev. B **67**, 195332 (2003).
[37] W. Ranke, Phys. Rev. B **41**, 5243 (1990).
[38] K. A. Feng, X. M. Hu, Z. Lin, and Y. R. Xing, Appl. Surf. Sci. **120**, 94 (1997).
[39] J. Wang, A. P. Horsfield, D. G. Pettifor, and M. C. Payne, Phys. Rev. B **54**, 13744 (1996).
[40] K. S. Kim, J. U. Choi, Y. J. Cho, and H. J. Kang, Surf. Interface Anal. **35**, 82 (2003).
[41] G.-D. Lee and E. Yoon, Phys. Rev. B **68**, 113304 (2003).
[42] H. Ikeda, Y. Oshima, H. Hirayama, and K. Takayanagi, Surf. Sci. **433-435**, 632 (1999).
[43] T. Suzuki, H. Minoda, Y. Tanishiro, and K. Yagi, Surf. Sci. **438**, 76 (1999).
[44] A. A. Stekolnikov, J. Furthmüller, and F. Bechstedt, Phys. Rev. B **68**, 205306 (2003).
[45] G.-H. Lu, M. Huang, M. Cuma, and F. Liu, Surf. Sci. **588**, 61 (2005).
[46] U. Myler, P. Althainz, and K. Jacobi, Surf. Sci. **251-252**, 607 (1991).
[47] L. Mantese, U. Rossow, and D. E. Aspnes, Appl. Surf. Sci. **107**, 35 (1996).
[48] U. Rossow, L. Mantese, and D. E. Aspnes, J. Vac. Sci. Technol. B **14**, 3070 (1996).
[49] C. D. Hogan and C. H. Patterson, Phys. Rev. B **57**, 14843 (1998).
[50] V. I. Gavrilenko and F. H. Pollak, Phys. Rev. B **58**, 12964 (1998).
[51] M. Palummo, G. Onida, R. DelSole, and B. S. Mendoza, Phys. Rev. B **60**, 2522 (1999).
[52] P. Hohenberg and W. Kohn, Phys. Rev. **136**, B864 (1964).
[53] http://www.abinit.org
[54] http://users.unimi.it/etsf
[55] W. Kohn and L. J. Sham, Phys. Rev. **140**, A1133 (1965).
[56] D. M. Ceperley and B. J. Alder, Phys. Rev. Lett. **45**, 566 (1980).
[57] J. P. Perdew and A. Zunger, Phys. Rev. B **23**, 5048 (1981).
[58] N. Troullier and J. L. Martins, Phys. Rev. B **43**, 1993 (1991).
[59] G. F. Bassani, *Electronic States and Optical Transitions in Solids* (Pergamon Press, Oxford, 1975).
[60] H. Ehrenreich and M. H. Cohen, Phys. Rev. **115**, 786 (1959).
[61] R. DelSole and R. Girlanda, Phys. Rev. B **48**, 11789 (1993).
[62] R. DelSole, in *Photonic Probes of Surfaces*, edited by P. Halevi (Elsevier, Amsterdam, 1995), p. 131.
[63] H. J. Monkhorst and J. D. Pack, Phys. Rev. B **13**, 5188 (1976).
[64] K. S. An, C. C. Hwang, H. S. Kim, C.-Y. Park, I. Matsuda, H. W. Yeom, S. Suga, and A. Kakizaki, Surf. Sci. **478**, 123 (2001).
[65] W. Arabczyk, H.-J. Mussig, J. Dąbrowski, D. Moszynski, and S. Hinrich, Appl. Surf. Sci. **135**, 59 (1998).
[66] C. Hogan, R. DelSole, and G. Onida, Phys. Rev. B **68**, 035405 (2003).
[67] I. Tamm, Phys. Z. Sowjetunion **1**, 733 (1932).
[68] K. C. Pandey, T. Sakurai, and H. D. Hagstrum, Phys. Rev. Lett. **35**, 1728 (1975).
[69] K. C. Pandey, J. Vac. Sci. Technol. **15**, 440 (1978).
[70] K. Gaál-Nagy and G. Onida, cond-mat/0611121; in *Epioptics-9*, edited by A. Cricenti (World Scientific, Singapore, to be published).
[71] A. Baldereschi, Phys. Rev. B **7**, 5212 (1973).
[72] R. DelSole and G. Onida, Phys. Rev. B **60**, 5523 (1999).
[73] C. Castillo, B. S. Mendoza, W. G. Schmidt, P. H. Hahn, and F. Bechstedt, Phys. Rev. B **68**, 041310(R) (2003).
[74] P. Monachesi, M. Palummo, R. DelSole, A. Grechnev, and O. Eriksson, Phys. Rev. B **68**, 035426 (2003).
[75] C. Hogan and R. DelSole, Phys. Status Solidi B **242**, 3040 (2005).
[76] K. Gaál-Nagy, A. Incze, G. Onida, Y. Borensztein, N. Witkowski, O. Pluchery, F. Fuchs, F. Bechstedt, and R. DelSole (unpublished).